

Semiconductor nanocrystals and embedded quantum dots: Electronic and optical properties

S. Schulz^{*,1}, S. Schumacher^{1,2}, and G. Czycholl¹

¹ Institute for Theoretical Physics, University of Bremen, P.O. Box 330440, 28334 Bremen, Germany

² Currently at: College of Optical Sciences, University of Arizona, Tucson, Arizona 85721, USA

Received 9 September 2006, accepted 21 September 2006

Published online 17 April 2007

PACS 68.65.Hb, 71.35.-y, 73.22.Dj, 78.67.Hc

A tight-binding model for semiconductor quantum dots (QD) consisting of a small gap semiconductor material A embedded within a larger gap material B is used to determine the bound, localized one-particle QD-states. The form and symmetry properties of these states and their dependence on form, size and composition of the QDs are discussed. The Coulomb and dipole matrix elements between these states are calculated so that a many-body Hamiltonian is derived describing the electronic properties of the QDs and the coupling to an applied (optical) electric field. Truncating the many-particle Hilbert space by taking into account only a finite number of localized electron and hole states the many-body Hamiltonian can be solved exactly. The resulting excitation spectrum and optical properties are presented and discussed. The method is, in particular, applied to CdSe QDs embedded in ZnSe with zincblende structure, to CdSe nanocrystals, and to InN QDs embedded in GaN with wurtzite structure. For the latter case also the influence of an intrinsic piezoelectric field and of the special symmetry properties of the wurtzite structure are discussed.

© 2007 WILEY-VCH Verlag GmbH & Co. KGaA, Weinheim

1 Introduction

A semiconductor quantum dot (QD) may be realized by means of colloidal chemical synthesis or by means of self organized clustering during the epitaxial growth process. In the former case the crystal growth in the environment of (mostly organic) surfactant material stops when the surface is covered by a monolayer of surfactant molecules, and a nanocrystal (NC) with a diameter of a few nm is created. The size and shape of the NCs can be controlled by external parameters (growth time, temperature, etc.). An embedded QD (EQD) may occur spontaneously in quantum well structures due to monolayer fluctuations in the well's thickness or self-assembled during epitaxial growth, when a material is grown on a substrate to which it is not lattice matched. Due to strain island formation on top of a two-dimensional "wetting-layer" (WL) may be energetically favorable (Stranski–Krastanov, SK-growth).

In this paper we describe a microscopic tight-binding (TB) method to determine the electronic properties of EQDs and NCs. The TB parameters of the pure semiconductor materials A and B are obtained by fitting the TB band structure to band structure properties known from experiment or from ab-initio calculations. Then an A-QD embedded within B-material is described by using the A-TB-parameters at the sites of the QD and the B-TB-parameters at all other sites. The effects of spin–orbit coupling, strain and piezoelectric fields can be incorporated into the TB model. Then the electronic one-particle states and eigenenergies of the A-QD are obtained by matrix diagonalization. The Coulomb and dipole matrix elements between these states can be calculated so that a many-body Hamiltonian for the QD coupled to an

* Corresponding author: e-mail: sschulz@itp.uni-bremen.de, Phone: +49-421-218 2965, Fax: +49-421-218 4869

external field is obtained, which is studied in a configuration interaction (CI) treatment. From the CI approach the optical properties of the QD can be obtained.

Here we give a short review on this TB method and on results obtained recently for different QD systems.

2 Theory

2.1 TB model for bulk materials

For the description of the bulk materials we start from an effective one-particle Hamiltonian in Wannier representation:

$$H^{\text{bulk}} = \sum_{R,R',n,m} t_{R-R',nm}^{(A,B)} |Rn\rangle \langle R'm| = \sum_k \sum_{\Delta} e^{ik\Delta} t_{\Delta,nm}^{(A,B)} |kn\rangle \langle km|. \quad (1)$$

We restrict the band indices n, m to the bands considered to be the most important ones for the electronic properties. This means that for the compounds CdSe and ZnSe with zincblende structure an $s_c p_a^3$ basis set is chosen, i.e. one s-orbital at the cation and three p-orbitals at the anion sites in each unit cell. The coupling of the basis orbitals is limited to nearest and next nearest neighbors Δ . Following Ref. [1], the spin-orbit component of the bulk Hamiltonian H^{bulk} couples only p-orbitals at the same atom. Now the different TB-parameters $t_{R-R',nm}$ are chosen so that the resulting TB bands reproduce the known values of the Kohn-Luttinger-Parameters ($\gamma_1, \gamma_2, \gamma_3$), the energy gap, the effective electron mass and the spin-orbit-splitting. Within this approach, the characteristic properties of the band structure in the region of the Γ -point are well reproduced. More details about the TB-model can be found in Ref. [2].

To reproduce the characteristic properties of the bulk band structures of wurtzite InN and GaN in the vicinity of the Γ -point, we use a TB-model with one s-state and three p-states per spin direction at each site inside the unit cell. Non-diagonal TB-matrix elements are included up to nearest neighbors Δ . The small spin-orbit coupling and crystal-field splitting are neglected. Then we are left with nine independent matrix elements. These matrix elements are again empirically determined so that the characteristic properties of the band structure around the Γ -point are well reproduced. More details are given in Ref. [3].

2.2 TB approach for embedded quantum dots (EQDs) and nanocrystals (NCs)

Starting from the bulk TB-parameters, the QD is modeled on an atomistic level, such that for each site the matrix elements are set according to the occupying atoms. For the nitrogen (N) or selen (Se) atoms at the interface between GaN and InN or CdSe and ZnSe, respectively, we use an averaged value for the on-site matrix elements. The valence band offset ΔE_v between the two materials (InN/GaN and CdSe/ZnSe, respectively) is included in our model by shifting the diagonal matrix elements of the bulk InN and CdSe, respectively. To model an embedded (InN or CdSe) QD in a barrier material (GaN or ZnSe), a finite zincblende or wurtzite lattice within a box is chosen. For the chemically synthesized CdSe nanocrystals (NCs), which are almost spherical in shape [4], the surface is passivated by organic ligands. Here the TB parameters, which describe the coupling between the dot material and the ligand molecules are simply chosen to be zero.

The resulting TB-Hamiltonian of the whole supercell corresponds to a finite but large matrix. For the matrix elements without the inclusion of strain effects the TB-parameters $t_{R-R',nm}$ of the bulk materials, determined as described in Section 2.1, are used. But in a heterostructure of two materials with different lattice constants, strain effects have to be included for a description of the electronic states, because the distance between two unit cells and the bond angles are not the same as the corresponding equilibrium values in the bulk. This means that the TB matrix elements $t_{R-R',nm}$ in the EQD differ from the matrix elements in the bulk material, if $R-R'$ is not the equilibrium distance of the bulk crystal. These strain effects are taken into account according to Harrison's d^{-2} rule [5].

The eigenstates and eigenenergies of the TB-Hamiltonian must be determined by efficient matrix diagonalization algorithms. For this purpose we employ the folded spectrum method (FSM) [6] combined with parpack routines.

2.3 Electrostatic built-in field

An electrostatic built-in field can significantly modify both the electronic and the optical properties of QDs. In contrast to cubic semiconductor heterostructures, the III–V wurtzite nitrides exhibit a considerably large built-in field [7]. In order to incorporate this field in the TB model for wurtzite structures, the electrostatic potential ϕ_p is determined from the solution of the Poisson equation and enters as a site-diagonal contribution $V_p(\mathbf{r}) = -e\phi_p(\mathbf{r})$ to the TB Hamiltonian [8]. In the case of wurtzite structures, the polarisation \mathbf{P} has two contributions, the spontaneous polarisation $\mathbf{P}^{\text{spont}}$ and the piezo-electric contribution $\mathbf{P}^{\text{piezo}}$ due to strain inside the system. For the latter we use the approximation described in Ref. [9] and assume $\mathbf{P}^{\text{piezo}} \sim \mathbf{e}_z$, which is well justified for the considered QD geometry [8].

3 Results for self assembled zincblende CdSe/ZnSe QDs

We consider a pyramidal QD, with base length $b = 10a$ (a : lattice constant of bulk ZnSe) and height $h = b/2$, on top of a one monolayer thick wetting layer (WL), grown in the (001)-direction. We have calculated the first five states for electrons and holes with and without including strain effects. To consider strain effects in our model the knowledge of the strain tensor ε is necessary, from which the new relative atomic positions $\mathbf{d}_{R'-R} = (1 + \varepsilon) \mathbf{d}_{R'-R}^0$ can be obtained. To appoint the strain tensor outside the EQD, the WL is treated as a quantum well [10]. The strain profile inside the EQD is obtained by using a model strain profile, which shows a similar behavior as the strain profiles of Ref. [11].

In Fig. 1(a) the isosurfaces of the squared electron and hole wavefunctions $|\Phi_i(\mathbf{r})|^2$ including strain effects are displayed. The red (light) and blue (dark) isosurface levels are selected as 0.1 and 0.5 of the maximum probability density, respectively. We obtain here, that the lowest electron state e_1 is an s-like state according to its nodal structure. The next two states e_2 and e_3 are p-like states. These states are oriented along the $[1\bar{1}0]$ and the $[110]$ direction, respectively, and splitted in energy due to the C_{2v} symmetry of the system. Obviously the hole states cannot be classified as being s-like (h_1), p-like (h_2 and h_3)

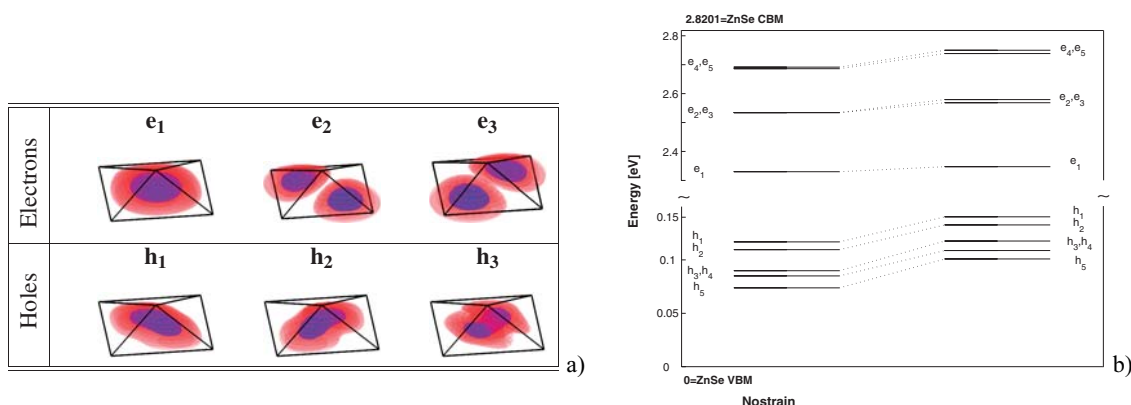


Fig. 1 (online colour at: www.pss-b.com) (a) Isosurfaces of the squared electron and hole wavefunctions with strain for the $b = 10a$ pyramidal QD. The light and dark surfaces correspond to 0.1 and 0.5 of the maximum probability density, respectively. (b) First five electron and hole state energies for the pyramidal CdSe QD. On the left-hand side the results for the unstrained QD are shown while on the right-hand side the results for the strained QD are displayed. The zero of the energy scale is the bulk ZnSe valence-band maximum (VBM). The energies are compared with the conduction-band minimum (CBM) of the bulk ZnSe.

or d-like (h_5) according to their nodal structures. With and without strain the hole states undergo a strong band mixing. Therefore the frequently used assumption of a single heavy-hole valence-band for the description of the bound hole states in a EQD even qualitatively yields incorrect results.

Figure 1(b) shows the comparison of the results for the strain-unaffected and strained pyramidal CdSe EQD. On the left-hand side of Fig. 1(b) the first five electron and hole-state energies for an unstrained EQD are displayed while the right-hand side shows the energies for the strained EQD. The lowest electron state is, by strain effects, shifted to higher energies. This is what one would expect for biaxial compression of the bulk material. The strain splits the states e_2 and e_3 further.

4 Results for zincblende CdSe NCs

In this section we investigate the single particle states of spherical CdSe NCs within our $s_c p_a^3$ TB-model. Due to the flexible surrounding matrix, these nanostructures are nearly unstrained [12] and their size is in between 10 and 40 Å in radius [4, 13, 14].

We model such a NC as an unstrained, spherical crystallite with perfect surface passivation. The zincblende structure is assumed for the CdSe NC. We neglect surface reconstructions [15] and concentrate on the size dependence of the results obtained for the electronic structure of the NCs.

We consider NCs of diameter between 1.82 nm and 4.85 nm. For the largest NCs (of diameter 4.85 nm) results for the four lowest lying electron and hole eigenstates are shown in Fig. 2 again in the form of an isosurface plot. The lowest lying electronic state e_1 obviously has spherical symmetry and can be classified as a 1s-state. Correspondingly the second state e_2 has the form of a 2s-state and the states $e_{3,4}$ are p-states. Despite the spherical symmetry of the system this simple classification is no longer possible for the hole states, however. Even the lowest lying hole state h_1 has no full rotational invariance, i.e. it cannot be classified as being an s-state. This is due to the intermixing of different atomic TB-valence states in the NC. Similarly the higher hole states h_2-h_4 cannot clearly be classified as an s- or p-like state. This is an effect, which simple effective mass models cannot account for, but which will have implications in the calculation of matrix elements between these states, which enter selection rules for optical transitions etc.

The discrete electronic states of semiconductor NCs are experimentally accessible by scanning tunneling microscopy (STM) [4, 13]. From these measurements the energy gap $E_{\text{gap}}^{\text{nano}}$ as well as the splitting Δ_{e_1, e_2} between electron ground state e_1 and the first excited state e_2 can be determined.

In Figure 3(a) we compare our TB-results for CdSe NCs with diameters in between 1.82 nm and 4.85 nm with STM results (dashed dotted line) and optical spectroscopy measurements (dotted line) [16]. The overall agreement with the TB results is very good, especially for the larger NCs. Deviations in the case of the small 2 nm NC arise from surface reconstructions [15] which are neglected here. When the same calculation is done without spin-orbit coupling (TB-NO SO), the energy gap $E_{\text{gap}}^{\text{nano}}$ is always

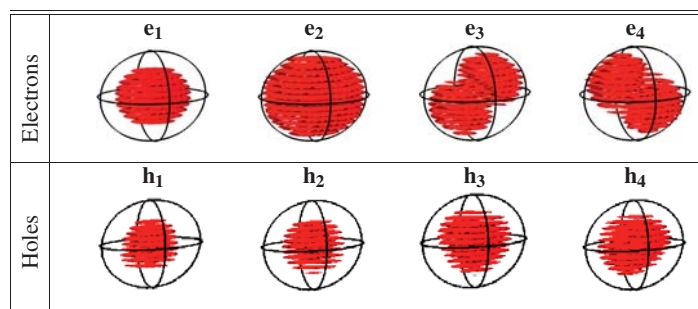


Fig. 2 (online colour at: www.pss-b.com) Isosurfaces (at 30% of the maximum probability density) of the squared electron and hole wavefunctions of spherical CdSe nanocrystals of diameter $d = 4.85$ nm for the four lowest states.

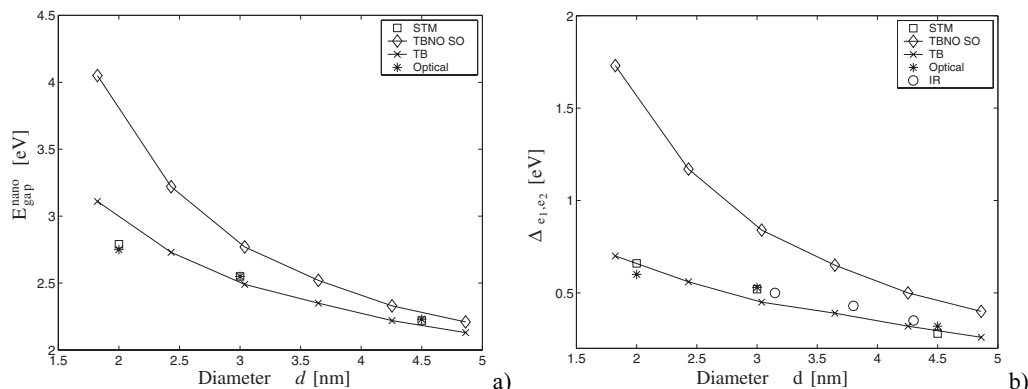


Fig. 3 (a) Energy gap $E_{\text{gap}}^{\text{nano}}$ as a function of the nanocrystal diameter d . Compared are the results from our TB-model with (TB) and without (TB-NO SO) spin-orbit coupling, a STM (STM) [13] and an optical measurement (Optical) [13]. (b) Splitting $\Delta_{e_1, e_2} = E_{e_2} - E_{e_1}$ between the lowest two electronic states as a function of the nanocrystal diameter d . The results from our TB-model, with (TB) and without (TB-NO SO) spin-orbit coupling, and from an STM measurement (STM, Ref. [13]) are displayed. Besides this results from infrared spectroscopy (IR, Ref. [17]) and optical methods (Optical, Ref. [13]) are shown.

strongly overestimated by the TB-model, in particular for smaller nanocrystals. So the spin-orbit coupling is important for a satisfactory reproduction of the experimental results.

Furthermore the calculated splitting $\Delta_{e_1, e_2} = E_{e_2} - E_{e_1}$ between the first two electron states e_1 and e_2 is compared with experimental results in Fig. 3(b) as a function of the nanocrystal diameter d . We have done the calculations again without (TB-NO SO) and with spin-orbit-coupling (TB). Without spin-orbit coupling the TB-model always overestimates the splitting Δ_{e_1, e_2} , but with spin-orbit coupling the results of the TB-model show good agreement with the experimental results.

5 Results for self assembled wurtzite InN/GaN QDs

In this section we consider a lens-shaped wurtzite InN QD, grown in the (0001)-direction on top of an InN wetting layer and embedded in a GaN matrix. Three different QDs with diameters $d = 4.5, 5.7, 7.7$ nm and heights of $h = 1.6, 2.3, 3.0$ nm, respectively, have been investigated. In a first approach we neglect the influence of the strain. In Fig. 4 we show the lowest lying bound electron and hole states of the smallest nitride QD. Due to the rotational symmetry of the QD in the hexagonal crystal structure we have here an exact degeneracy of the e_2 - and e_3 -electron as well as of the h_2 - and h_3 -hole states. Otherwise we observe again that the hole states cannot be simply classified as s- or p-like states according to their symmetry due to band mixing effects of the valence bands.

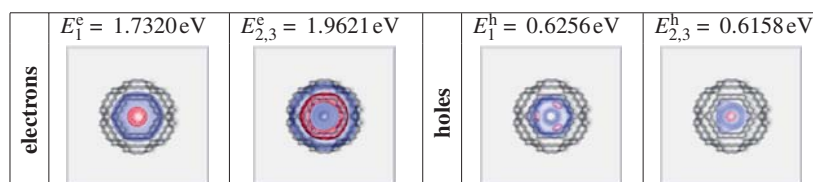


Fig. 4 (online colour at: www.pss-b.com) QD structure shown from atop. Isosurfaces of the probability density with 20% (blue) and 80% (red) of the maximum value are shown. Depicted are the first two bound shells for electrons (left) and holes (right). Only one state is visualized for the two-fold degenerate p-shell, as the other one looks alike. The corresponding energies ($E_{1,2,3}^{e,h}$) are measured relative to the valence band maximum of the bulk GaN.

Under the influence of the electrostatic built-in field, the electron single-particle states are shifted towards the top of the QD whereas the hole states move to the bottom of the nanostructure. In case of the largest QD, a clear spatial separation of electron and hole wave functions is observed. This leads to a decrease in the dipole matrix elements. For the intermediate and largest QD with built-in field, the hole ground state is formed by the two degenerate states Φ_1^h and Φ_2^h (p-shell) whereas the first excited state Φ_3^h (s-shell) is nondegenerate. This behavior is interchanged with decreasing QD size, and for the smallest QD, the ground state is formed by the s-shell, see Fig. 4.

From the one particle states presented above an effective many body Hamiltonian can be obtained:

$$H = H_0 + H_C + H_D, \quad (2)$$

where

$$H_0 = \sum_i \varepsilon_i^e e_i^\dagger e_i + \sum_i \varepsilon_i^h h_i^\dagger h_i$$

is the one-particle part (being diagonal with respect to the calculated QD eigenstates),

$$H_C = \frac{1}{2} \sum_{ijkl} V_{ij,kl}^{ee} e_i^\dagger e_j^\dagger e_k e_l + \frac{1}{2} \sum_{ijkl} V_{ij,kl}^{hh} h_i^\dagger h_j^\dagger h_k h_l - \sum_{ijkl} V_{ij,kl}^{he} h_i^\dagger e_j^\dagger e_k h_l \quad (3)$$

describes the Coulomb interaction and

$$H_D = \sum_{i,j} (e \langle i | \mathbf{E} \mathbf{r} | j \rangle e_i h_j + \text{h.c.}) \quad (4)$$

denotes the coupling to an external field \mathbf{E} in dipole approximation. In the spirit of a TB-model and its assumptions we approximate the Coulomb matrix elements by:

$$V_{ijkl} = \sum_{\mathbf{R}\mathbf{R}'} \sum_{\alpha\beta} c_{\mathbf{R}\alpha}^{i*} c_{\mathbf{R}'\beta}^{j*} c_{\mathbf{R}'\beta}^k c_{\mathbf{R}\alpha}^l V(\mathbf{R} - \mathbf{R}'), \quad (5)$$

with

$$V(\mathbf{R} - \mathbf{R}') = \frac{e_0^2}{4\pi\varepsilon_0\varepsilon_r |\mathbf{R} - \mathbf{R}'|} \quad \text{for } \mathbf{R} \neq \mathbf{R}',$$

and

$$V(0) = \frac{1}{V_{uc}^2} \int_{uc} d^3r d^3r' \frac{e_0^2}{4\pi\varepsilon_0\varepsilon_r |\mathbf{r} - \mathbf{r}'|} \approx V_0. \quad (6)$$

The operator \mathbf{r} is approximated by $\mathbf{r} = \sum_{\mathbf{R}\alpha} |\mathbf{R}, \alpha\rangle \mathbf{R} \langle \mathbf{R}, \alpha| + \sum_{\mathbf{R}\alpha} \sum_{\mathbf{R}'\beta} |\mathbf{R}, \alpha\rangle \langle \mathbf{R}, \alpha| \tilde{\mathbf{r}} |\mathbf{R}', \beta\rangle \langle \mathbf{R}', \beta|$, where $\tilde{\mathbf{r}}$

denotes positions within a unit cell relative to \mathbf{R} . The expansion coefficients $c_{\alpha,\mathbf{R}}^i$ are related to the i -th one-particle wave function $\Phi_i(\mathbf{r}) = \sum_{\alpha,\mathbf{R}} c_{\alpha,\mathbf{R}}^i \phi_{\alpha,\mathbf{R}}(\mathbf{r})$ where $\phi_{\alpha,\mathbf{R}}(\mathbf{r})$ denotes the atomic wave functions localized at the lattice site \mathbf{R} .

With the determined dipole and Coulomb matrix elements and the resulting many-body Hamiltonian the calculation of optical spectra can directly be performed as described in Ref. [18]. To keep the discussion simple, we included only the first three bound electron and hole states in a configuration-interaction (CI) calculation [18]. The excitonic absorption and emission spectra, calculated by Fermi's golden rule, are depicted for the smallest and the largest QD in Fig 5. The excitonic absorption for the small QD with (solid line) and without (dashed line) the built-in field is shown in Fig. 5(a). According to the dipole selection rules, the lower energy line is dominated by contributions where the electron is excited in the

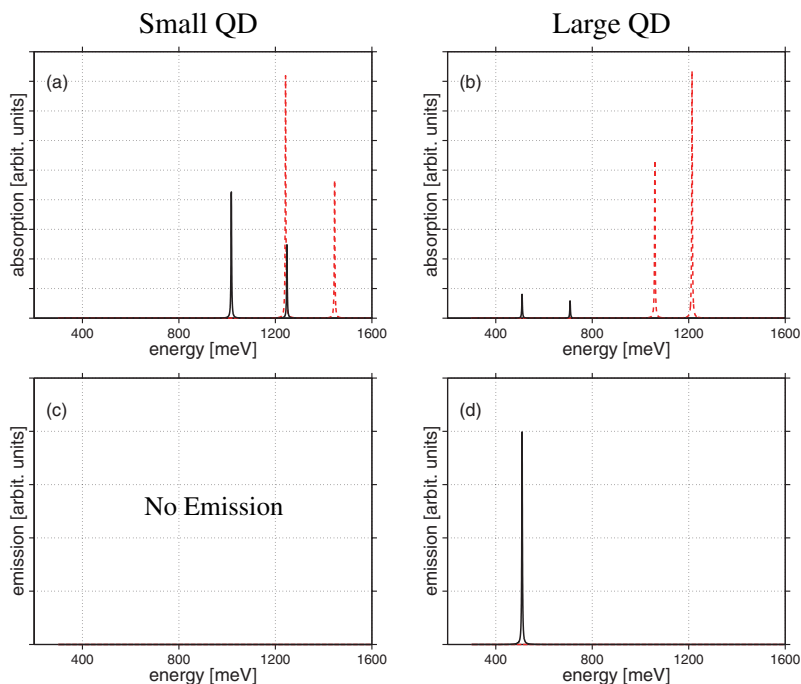


Fig. 5 (online colour at: www.pss-b.com) (a) Excitonic absorption for the small QD with (solid line) and without (dashed line) the influence of the built-in field. (b) Same as (a) but for the large QD. Excitonic ground state emission for the small (c) and the large (d) QD with the influence of the built-in field. Without the built-in field, the ground state emission also vanishes for the large QD and is consequently not shown.

s-shell and the hole in the p-shell, and vice versa for the high energy line. Under the influence of the built-in field, the whole spectrum is red-shifted. In addition, the built-in field leads to a spatial separation of electron and hole wave functions and therefore the oscillator strengths are drastically reduced. For the small QD no exciton ground state emission is observed, as discussed in detail in Ref. [19] and shown in Fig. 5(c). Figure 5(b) shows the excitonic absorption spectrum with (solid line) and without (dashed line) the built-in field for the large QD. Compared to the small QD, the separation of electron and hole wave functions is much more pronounced and therefore the reduction of the oscillator strength and the redshift in energy is much larger. For the large QD with the built-in field the ground state is a two-fold degenerate state (*p*-shell). Therefore the main contribution to the exciton ground state is formed by the electron in the s-shell, and the hole in the p-shell. In contrast to the small QD, a nonvanishing exciton ground state emission can be observed, which is depicted in Fig. 5(d). Without the built-in field no emission is observed.

6 Conclusion

We have shown that an empirical tight-binding model is suitable for a realistic microscopic modelling of the electronic properties of semiconductor embedded quantum dots and nanocrystals. Starting from the TB-parameters, which well reproduce the bulk band structure, the nanostructures can be modelled taking realistically into account effects like strain, spin-orbit coupling, built-in electric fields, etc. From the obtained one-particle states the Coulomb and dipole matrix elements and therefore a many-body Hamiltonian with a coupling to an external field can be derived, from which optical spectra can be calculated.

Acknowledgements The authors acknowledge financial support by the Deutsche Forschungsgemeinschaft and a grant for CPU time from the John von Neumann Institute for Computing at the Forschungszentrum Jülich.

References

- [1] D. J. Chadi, *Phys. Rev. B* **16**, 790 (1977).
- [2] S. Schulz and G. Czycholl, *Phys. Rev. B* **72**, 165317 (2005).
- [3] S. Schulz, S. Schumacher, and G. Czycholl, *Phys. Rev. B* **73**, 245327 (2006).
- [4] U. Banin, C. Yun Wei, D. Katz, and O. Millo, *Nature* **400**, 542 (1999).
- [5] S. Froyen and W. A. Harrison, *Phys. Rev. B* **20**, 2420 (1979).
- [6] L.-W. Wang and A. Zunger, *J. Chem. Phys.* **100**, 2394 (1994).
- [7] F. Bernardini, V. Fiorentini, and D. Vanderbilt, *Phys. Rev. B* **56**, R10024 (1997).
- [8] T. Saito and Y. Arakawa, *Physica E (Amsterdam)* **15**, 169 (2002).
- [9] S. D. Rinaldis, I. D'Amico, and F. Rossi, *Phys. Rev. B* **69**, 235316 (2004).
- [10] S. L. Chuang, *Physics of Optoelectronic Devices* (Wiley-Interscience Publication, New York, 1995).
- [11] O. Stier, M. Grundmann, and D. Bimberg, *Phys. Rev. B* **59**, 5688 (1998).
- [12] A. P. Alivisatos, *Science* **271**, 933 (1996).
- [13] B. Alpers, I. Rubinstein, G. Hodes, D. Porath, and O. Millo, *Appl. Phys. Lett.* **75**, 1751 (1999).
- [14] B. S. Kim, M. A. Islam, L. E. Brus, and I. P. Herman, *J. Appl. Phys.* **89**, 8127 (2001).
- [15] S. Pokrant and K. B. Whaley, *Eur. Phys. J. D* **6**, 255 (1999).
- [16] A. I. Ekimov, F. Hache, M. C. Schanne-Klein, D. Ricard, C. Flytzanis, I. A. Kudryavtsev, T. V. Yazeva, A. V. Rodina, and A. L. Efros, *J. Opt. Soc. Am. B* **10**, 100 (1993).
- [17] P. Guyot-Sionnest and M. A. Hines, *Appl. Phys. Lett.* **72**, 686 (1998).
- [18] N. Baer, P. Gartner, and F. Jahnke, *Eur. Phys. J. B* **42**, 231 (2004).
- [19] N. Baer, S. Schulz, S. Schumacher, P. Gartner, G. Czycholl, and F. Jahnke, *Appl. Phys. Lett.* **87**, 231114 (2005).